Recognition determinants of broad and potent HIV-1 neutralization by an affinity matured antibody from a pediatric elite-neutralizer

Sanjeev Kumar[1,2,†], Swarandeep Singh[1,†], Arnab Chatterjee[3,†], Prashant Bajpai[2], Shaifali Sharma[1], Sanket Katpara[1], Rakesh Lodha[4], Somnath Dutta[3,*], Kalpana Luthra[1,*]

[1]Department of Biochemistry, All India Institute of Medical Sciences, New Delhi, India
[2]ICGEB-Emory Vaccine Center, International Center for Genetic Engineering and Biotechnology, New Delhi, India
[3]Molecular Biophysics Unit, Indian Institute of Science, Bangalore, India
[4]Department of Pediatrics, All India Institute of Medical Sciences, New Delhi, India

[†]Equal contribution

[*]Correspondence

E-mail: kalpanaluthra@gmail.com, somnath@iisc.ac.in

Keywords

HIV-1, clade-C, N332 supersite, pediatric HIV-1 bnAb, elite-neutralizer, SOSIP trimer, Cryo-EM structure

ABSTRACT

The structural and characteristic features of HIV-1 broadly neutralizing antibodies (bnAbs) from chronically infected pediatric donors are currently unknown. Herein, we characterized a heavy chain matured HIV-1 bnAb 44m, identified from a pediatric elite-neutralizer. Interestingly, in comparison to its wild-type AIIMS-P01 bnAb, 44m exhibited moderately higher level of somatic hypermutations (SHM) of 15.2%. 44m neutralized 79% of HIV-1 heterologous viruses tested, with a geometric mean IC_{50} titer of 0.36 μg/ml. The cryoEM structure of 44m Fab in complex with fully-cleaved glycosylated native-like BG505.SOSIP envelope trimer at 4.4 Å resolution revealed that 44m targets the V3-glycan N332-supersite and GDIR motif to neutralize HIV-1 with improved potency and breadth, plausibly attributed by a matured heavy chain as compared to that of wild-type AIIMS-P01 bnAb. This study improves our understanding on pediatric HIV-1 bnAbs and

structural basis of broad HIV-1 neutralization by 44m may be useful blueprint for vaccine design in future.

INTRODUCTION

Extensive efforts are currently ongoing worldwide to develop a safe and effective vaccine to human immunodeficiency virus-1 (HIV-1). During HIV-1 infection, neutralizing antibodies (nAbs) are elicited against the envelope (env) glycoprotein gp160[1,2]. Highly potent broadly neutralizing antibodies (bnAbs) are found to develop and evolve in only top 1% of HIV-1 infected individuals, classified as elite-neutralizers[3,4]. So far, seven distinct epitopes of HIV-1 bnAbs have been identified to be present on the viral env that are: V2-apex, V3-glycan N332-supersite, CD4 binding site (CD4bs), silent-face center (SFC), membrane-proximal external region (MPER), gp120–gp41 interface and fusion peptide (FP)[1]. Presently, the prime goal is to design and develop an HIV-1 vaccine capable of triggering naïve B cells and steer them to evolve into bnAb generating B cells upon immunization/vaccination[5–7].

HIV-1 infected infants have been shown to develop bnAb responses within one year of age[8,9]; while in infected adults, it takes at least 2 to 3 years post infection for the development of bnAbs[3,10,11], suggesting distinct maturation pathways of the bnAbs evolving in children[8,12]. The HIV-1 bnAbs isolated from adults have been extensively characterized, both structurally and functionally; with some of them exhibiting characteristic features of high somatic-hypermutations (SHM) and long CDR3 regions[1], while there is a paucity of such information on the bnAbs generated by HIV-1 infected children. A number of studies carried out on HIV-1 infected pediatric cohorts have reported HIV-1 plasma bnAb responses targeted at multiple env epitopes including the V2-apex, N332-glycan supersite, CD4bs and MPER[8,9,13–17]; however isolation of only two pediatric HIV-1 bnAbs have been reported thus far: BF520.1 by Simonich et al[9] and AIIMS-P01 by us[18]. Binding of both AIIMS-P01 and BF520.1 are dependent on the N332-supersite epitope present at the base of the V3-glycan region[9,18]. Both pediatric bnAbs exhibit limited SHM (~7%); however, there is paucity of information towards understanding whether an increased SHM can be acquired in bnAbs evolving in HIV-1 infected children and further, if the increased SHM in pediatric bnAbs can lead to increase

58 in their potency and breadth of viral neutralization, as observed in bnAbs evolving in HIV-
59 1 infected adults[1,2,19–28].

60 Immunogenetic information of HIV-1 bnAbs from adults and children obtained from deep
61 sequencing or single cell analysis of B cell repertoire (BCR) can further our
62 understanding of their natural development during the course of infection and
63 development of blueprints for rational vaccine design and effective vaccination
64 strategies[5,6]. Furthermore, structural characterization of potent bnAbs, in complex with
65 native-like trimeric env can provide useful mechanistic insights for broad and potent
66 neutralization of HIV-1 heterologous viruses.

67 We previously reported the isolation of a bnAb AIIMS-P01, from an antiretroviral naïve
68 HIV-1 clade-C chronically infected pediatric elite-neutralizer AIIMS_330[15,16,18,29,30].
69 Herein, to delineate the characteristics of an affinity matured lineage member antibody
70 of the AIIMS-P01 pediatric bnAb, we performed the structural and functional
71 characterization of a heavy chain matured pediatric HIV-1 AIIMS-P01 bnAb lineage
72 monoclonal antibody clone 44m (referred to as 44m). The 44m exhibited moderate level
73 of SHM (15.2%) and demonstrated near about 80% HIV-1 neutralization breadth with
74 ~2 times improved potency than AIIMS-P01 wild-type (WT) bnAb. CryoEM analysis of
75 44m in complex with BG505.SOSIP trimer revealed structural insights for broad HIV-1
76 neutralization.

77 **RESULTS**

78 **Identification of a matured AIIMS-P01 lineage antibody**

79 We previously reported the isolation and characterization of a broad and potent anti-HIV-
80 1 bnAb AIIMS-P01 from an Indian clade-C infected pediatric elite-neutralizer
81 AIIMS_330[18]. To understand the role of affinity matured AIIMS-P01 antibody in HIV-1
82 neutralization, we performed the deep sequencing of bulk B cell repertoire from total
83 peripheral blood mononuclear cells (PBMCs) of the AIIMS_330 pediatric elite-neutralizer
84 (Kumar S et. al. unpublished data). We identified 21 heavy chain sequences that matched
85 the CDRH3 sequence of AIIMS-P01, with varied and moderate level (30 nt – 47 nt) of
86 antibody somatic hypermutations (SHM) (**Fig. S1**). We did not find matched CDRL3 light
87 chain genes as that of the AIIMS-P01. As observed by us previously, the heavy chain

88 dominantly contributed to HIV-1 neutralization breadth[18]. Therefore, to understand the
89 effect of higher level of SHM in matured AIIMS-P01 lineage members, herein, we
90 synthesized a matured (15.2% SHM) AIIMS-P01 bnAb heavy chain gene with >85%
91 similar CDRH3 sequence as of AIIMS-P01, designated as 44m and expressed the mAb by
92 co-transfecting plasmids carrying this heavy chain gene and the WT AIIMS-P01 light
93 chain gene.

94 **Matured AIIMS-P01 lineage antibody 44m showed improved breadth and potency**
95 **than AIIMS-P01**

96 We first determined the binding reactivity of the matured 44m monoclonal antibody to
97 heterologous HIV-1 monomeric and trimeric envelope proteins and observed high
98 binding efficiency (**Fig. 1a**). To further validate the binding data obtained by ELISA,
99 affinity analysis of the 44m with HIV-1 SOSIP trimer was performed using Octet BLI
100 assays. Antibody 44m showed high nanomolar (nM) affinity (KD: 0.56 nM) with
101 BG505.SOSIP.664 T332N (**Fig. 1b**). The neutralization potential of 44m mAb was tested
102 against heterologous viruses and the global panel of HIV-1 viruses, at concentrations
103 ranging from 10μg/ml to 0.001 μg/ml, using a TZM-bl based neutralization assay[31]. The
104 44m bnAb neutralized 77% HIV-1 clade-C viruses and 80% clade-B viruses and
105 demonstrated an overall improvement of breadth of 79% against the heterologous
106 viruses tested, and potency, with a geometric mean IC_{50} titer of 0.36 μg/ml, as compared
107 to that of AIIMS-P01. Further, a 58% breadth, with IC_{50} titer of 0.43 μg/ml was observed,
108 on testing this bnAb against the global panel of viruses (**Fig. 2**). The neutralizing activity
109 data reveal an increase in potency and breadth of the matured version 44m against the
110 heterologous viruses tested and increased SHM in comparison to AIIMS-P01 WT (**Fig. 1c,**
111 **d**). These findings encouraged us to perform structural characterization of 44m antibody
112 with the stabilized envelope BG505.SOSIP.664 T332N.

113 **44m targets the V3 loop of Env and showed binding dependence on the GDIR Motif**

114 Structural insight into mature 44m bnAb binding in the context of BG505.SOSIP a natively
115 glycosylated Env was achieved by Cryo-Electron microscopy. The 44m bnAb Fab and
116 BG505.SOSIP Env trimer were expressed and purified from Expi293F cells which include
117 similar glycoforms as Env trimers expressed in human cells. We solved the structure with
118 a global resolution of 4.4 Å and local resolution of 3.36 Å and 3.74 Å (**Fig. 3 and S2 – S5)**.

119 The atomic model fitted in the EM map of BG505 trimer in complex with Fab of the
120 44m bnAb displayed a total of three 44m Fabs, with one Fab bound to each protomer of
121 the Env trimer for effective neutralization (**Fig. 3**). Cryo-EM structures of BG505.SOSIP
122 Env trimer with 44m bnAb indicated trimeric shapes of HIV trimer, which additionally
123 connected with extra densities, attributed to the corresponding bound Fab moieties (**Fig.**
124 **S2b**). Different subdomains, gp120, gp41 and Fab densities were visible in the high-
125 resolution cryo-EM structure of the Env trimer in complex with 44m bnAb (**Fig. 3**).

126 Structural analysis revealed that the CDRH3 loop of neutralizing antibody 44m stretched
127 deep inside the groove between the N295 and N332 residues, thus reaching the base of
128 the V3 loop of gp120 and established a range of chemical bonds with the nearby favorable
129 amino acids (**Fig. 4a**). The total occupied surface area of 44m is ~750 $Å^2$, with extensive
130 participation of the heavy chain. This surface area includes all the CDR regions and FR3
131 region, but the CDRH1 and CDRH3 loop show a predomination contribution. The
132 positioning of the CDR regions of the heavy chain is crucial to establish contact points
133 with the V3 loop of the gp120 **(Fig. 4a, b).** The key residues on the CDRH3 loop that are
134 interacting with the gp120 region are V106, P107, A 108, R109, and W110, whereas the
135 primary contact points of CDRH1 and CDRH2 loops with the CD4bs are H31, Y52, Y53,
136 T54, D56, and T57 **(Fig. 4b)**. These interactions are mainly stabilized by both hydrogen
137 bonding and van der Waals interactions. Interestingly, the R109 residue of the CDRH3
138 demonstrated a salt bridge interaction with the D325 site of the gp120 region **(Fig. 4c)**.
139 These interacting residues are hidden within the different clefts of the V3 loop of the
140 gp120 region. The surface potential map of the paratope region depicts the interacting
141 residues of CDR regions placed near the polar residues of the V3 loop **(Fig. 4d and S6)**.

142 **44m interacts with N332-supersite**

143 The antibody-Env protein interaction studies unraveled the possibilities to explore the
144 glycan antibody interactions. The atomic model demonstrated that the interaction sites
145 for 44m bnAbs on gp120 were positioned in an area that is surrounded by three N-glycan
146 patches: the Asn301, Asn332 located near the base of V3, the Asn156 glycan in the V1V2
147 region, and the Asn295 glycan near the bottom of gp120 **(Fig. 5a-d)**. This binding
148 approach created an interlocked system of V_H loop of 44m and V3 loops of gp120, and
149 forming a stable antibody-antigen complex **(Fig. 5b).** Glycan binding to N301 is forming

150 contacts with polar and charged amino acids of the CDRH2 loop, wherein the T54 and
151 D56 of the CDRH2 region are interacting with the polar side of glycan moieties to mask
152 the binding to host cells **(Fig. 5c)**. The N332 glycan engages in forming the largest
153 interacting area, with most of the CDRH3 region involving different portions of glycan
154 moieties on it. N-Acetyl glucosamine attached to the N332 residue is forming hydrogen
155 bonding with Ser111 and Tyr113 residues of the CDRH3 region **(Fig. 5d).** The structural
156 analysis showed that the 44m antibody interacts with different glycan moieties attached
157 to asparagine residues at 301 and 332 positions in the V3 region.

158 **44m showed distinct glycan binding interactions, with similar pattern of epitope**
159 **interaction like other V3-glycan bnAbs**

160 A comparative structural analysis of the 44m antibody with other available bnAbs (BG18,
161 10-1074, DH270.6 & BF520.1) was performed to understand the exceptionality of this
162 44m antibody **(Fig. S6 - S8)**. Superimposition of the antibodies directed at the V3 loop
163 region of the gp120 protomer showed a common interaction pattern across all the bnAbs
164 within the V3 region. In the BG18 bnAb (6dfg) CDRL3 and CDRH3 loops are interacting
165 with V3 region for stalking of the antibody onto the gp120 (**Fig. S8a**). In bnAb 10-1074
166 (6udj), the V3 loop of gp120 protomer interacts with CDRH3 and CDRL3 regions (**Fig.**
167 **S8b**). DH270.6 (6um6) and BF520.1 (6mn7) have more inter-facial area**,** which helps in
168 the interaction of residues in CDRL1 and CDRL2 regions. Additionally, the V1 region
169 interacts with the CDRL3 loop (**Fig. S8c, d**). The V3 loop has stable bonding with the
170 CDRH1 loop for effective neutralization. The presence of an 8 amino acid long elongated
171 face in the CDRH3 region in PGT121 and PGT122 classes of antibodies make these
172 antibodies potent to bind gp120 surface using two functional surfaces (**Fig. S8e**). These
173 results suggest that the overall binding region of the CDR with both V3 and V1/V2 loops
174 were significantly increased. The superimposition of V3-glycan bnAbs into the gp120
175 trimer depicts the variability in the binding surface area but a common binding pattern
176 on the gp120.

177 **44m HIV-1 bnAb showed co-dependence on GDIR motif and N332-supersite**

178 Results obtained from structural mapping of 44m showed that this bnAb binds the N156,
179 N295, N301, D325 residue of GDIR motif and N332-supersite env regions **(Fig. 3c & 4b)**.
180 Next, we used this structural mapping information to understand the linkage of these

181 residues in 44m mediated HIV-1 neutralization by performing sequence alignment of
182 these identified contact residues within the envelope regions of the viruses tested. The
183 analysis revealed that the N156 and N301 glycans are relatively conserved whereas
184 mutations at the N295 residue are present heterogeneously among the 44m resistant and
185 susceptible viruses, suggesting these mutations may not be majorly contributing to the
186 44m mediated viral neutralization (**Fig. S9**). In contrast, mutations present at D325 and
187 N332 positions were found to be associated with abrogation in neutralization potential
188 of 44m and vice-versa, e.g. HXB2, ZM249 and ZM233 viruses were resistant to
189 neutralization by 44m, due to the absence of GDIR epitope in these viruses. These findings
190 suggest that the neutralization dependence of the pediatric bnAb 44m relies on the D325
191 residue of GDIR motif and N332-spersite, as has also been reported for the adult HIV-1
192 V3 bnAbs PGT121 and 10-1074.

193 **DISCUSSION**

194 The footprints of HIV-1 broadly neutralizing antibodies (bnAbs) can provide a template
195 for structure-guided vaccine design[5,6]. Highly potent bnAb based therapeutics,
196 prophylactics and vaccines are attractive strategies to tackle HIV-1[1]. Immunogenetics
197 based information of potent HIV-1 bnAbs derived from deep sequencing or single cell
198 analysis of B cell repertoire (BCR) of infected donors can provide critical insights towards
199 understanding their natural development during the course of infection and reveal the
200 frequency of B cells within the human B cell repertoire, that can elicit potent bnAbs to
201 guide vaccination strategies[5,25,32,33]. Further, the structural characterization of potent
202 HIV-1 bnAbs in complex with the viral envelope provides useful mechanistic insights of
203 viral neutralization and information of epitope-paratope interaction for rational vaccine
204 design[6]. Currently, the leading strategy in innovative HIV-1 next-generation
205 immunotherapeutic and vaccine design is to develop and elicit bnAb responses by
206 steering bnAb expressing B cells[5,7]. To achieve this goal, it is essential to understand the
207 structural mechanism of HIV-1 neutralization and immunogenetics of B cells that elicit
208 potent bnAbs. The evolution of HIV-1 bnAbs from adult donors has been studied
209 extensively[25,34,35], but, no information is available on the evolving HIV-1 bnAb lineage in
210 chronically infected children.

211 Herein, to fill this knowledge gap, we synthesized a heavy chain matured lineage member
212 of AIIMS-P01 bnAb and evaluated its structural features and functionality in terms of viral
213 binding and neutralization activity. We used only heavy chain of AIIMS-P01 matured
214 lineages as we didn't find matched CDRL3 of the AIIMS-P01 light chain in our deep
215 sequencing data (unpublished), plausibly due to the low depth of sequencing. We
216 combined functional and structural approaches and showed that maturation in the 44m
217 heavy chain, like that reported for the adult bnAbs of the PGT class[34,36], was functionally
218 important for HIV-1 Env binding and neutralization. This was demonstrated by the
219 increased heterologous breadth observed when the mature heavy chain was paired with
220 the original light chain of AIIMS-P01 WT bnAb, suggesting that the recently acquired
221 SHMs can be functionally important for the evolution and neutralization breadth for this
222 bnAb. In addition, the matured bnAb 44m exhibited a change of indel sequence (SNPSR
223 mutated to SDPIR**,** in comparison to its WT bnAb AIIMS-P01 **(Fig. 4e)**, specifically from
224 non-polar residues to acidic & hydrophobic residues, which plausibly creates an
225 electronegativity that could enhance the contact of antibody loops with the virus.

226 Unlike HIV-1 CD4bs bnAbs, the V3-glycan targeting bnAbs are of high interest because
227 they are common and not restricted by certain germline genes[1,2]. The pediatric bnAb
228 AIIMS-P01 and infant derived BF520.1 are of particular interest because these showed
229 broad HIV-1 neutralization despite limited SHM[9,18]. The 44m lineage bnAb identified and
230 characterized herein showed improved neutralization potency and breadth plausibly by
231 acquisition of higher number of SHM, that led to an increase in potency twice that of the
232 WT AIIMS-P01 bnAb. The Cryo-EM structural analysis of bnAb 44m, indicated that
233 CDRH1 (H31, Y53 and T57) and CDRH3 (P107, A108 and R109) residues appear to
234 contribute to the 44m paratope by mediating contacts with the conserved V3-glycan
235 N332-supersite, D325 of 'GDIR' sequence motif, glycans at position 137, 156, 295, 301
236 and 332. These major determinants of neutralization breadth interacting with residues
237 within the CDRH1 and CDRH3 regions of the 44m, similar to that in the adult bnAbs and
238 distinct from the infant bnAb BF520.1[9,34]. The angle of approach by 44m towards the V3
239 epitope was previously determined to be similar to PGT121[37,38], although the positioning
240 of 44m was notably different and slightly rotated relative to the PGT121. The crystal
241 structure of PGT121 in complex with gp120 identified the GDIR motif and glycans at
242 positions N332 and N301 as the primary contacts defining the PGT121 epitope[37,38]. The

243 CDRH3 loop, which is highly mutated in PGT121, penetrates the glycan shield in order to
244 contact both the GDIR motif and N332 glycan.

245 The structural model similarly indicates potential CDRH3 contacts with the GDIR motif
246 and N332 glycan. However, structurally defined epitope-paratope interface do not fully
247 capture the functional binding contacts that drive neutralization and escape[39],
248 reinforcing the gravity of functional assays to define the recognition determinants that
249 are important for neutralization activity. Though we observed that 44m interacts with
250 other V3-region glycans including N295 and N301, however, HIV-1 viral sequence
251 alignment revealed that 44m is primarily dependent on N332-glycan supersite and GDIR
252 motifs. Based on the findings of HIV-1 binding, neutralization and structural analysis of
253 the 44m pediatric bnAb, we postulate that a germline targeting vaccine / immunogen
254 could easily elicit AIIMS-P01 / 44m-like responses. In the AIIMS_330 pediatric elite
255 neutralizer, the circulating and coevolving viruses may have led to elicitation of this bnAb
256 lineage (44m), to drive affinity maturation in the AIIMS-P01 bnAb, as has been observed
257 previously for the evolution of V1V2 and V3-glycan plasma bnAbs[15].

258 In summary, the structural and functional characterization of a heavy chain matured
259 pediatric bnAb 44m showed improved HIV-1 neutralization potency and breadth in
260 comparison to its WT bnAb AIIMS-P01. This study for the first time provides an evidence
261 towards contribution of antibody SHM in improved HIV-1 neutralizing efficiency of a
262 pediatric bnAb. Further studies in this direction are required to be conducted to
263 understand the antigenic triggers in chronically infected children that can elicit similar
264 protective bnAbs targeting other HIV-1 bnAb epitopes which in turn can provide simpler
265 blueprint to guide HIV-1 vaccine design.

266 **METHODS**

267 **Ethics statement**

268 This study was conducted after obtaining approval from the institutional ethics
269 committee, All India Institute of Medical Sciences (AIIMS), New Delhi, India (IEC/-
270 532/1111.2016 & IEC-72/01.02.2019).

271 **Antibody gene synthesis**

272 The antibody heavy chain genes of matured AIIMS-P01 lineage antibody was synthesized
273 after codon-optimization for mammalian expression from Genscript, Inc. USA, and cloned
274 in respective monoclonal antibody expression vector AbVec under AgeI and SalI sites[40].

275 **Antibody genes sequence analysis**

276 The sequencing of the antibody genes was done commercially from Eurofins, India. The
277 sequences were analyzed online through IMGT/V-QUEST
278 (http://www.imgt.org/IMGT_vquest/vquest)[41].

279 **Expression of monoclonal antibodies**

280 All HIV-1 mAbs were expressed in Expi293F cells (Thermo Fisher) as described
281 previously[18,42]. Briefly, 15µg each of heavy chain and light chain expressing IgG1 plasmids
282 were co-transfected using PEI-Max as transfection reagent. Following 4-6 days of
283 incubation, cells were harvested by centrifugation and filtered through 0.22 mm syringe
284 filter (mdi). The supernatant was added to a Protein A column affinity chromatography
285 column (Pierce). The column was then washed with 1×PBS and mAbs were eluted with
286 IgG Elution Buffer (Pierce), immediately neutralized with 1M Tris pH 8.0 buffer and
287 extensively dialyzed against 1×PBS at 4°C. The mAbs were then concentrated using
288 10kDa Amicon Ultra-15 centrifugal filter units (EMD Millipore), filtered through a 0.22
289 mm syringe filter (mdi) and stored at -80°C for further use.

290 **Expression and purification of BG505.SOSIP.664 T332N trimeric proteins**

291 The BG505.SOSIP.664.C2 T332N gp140 trimeric proteins with twin-strep-tag was
292 expressed in HEK 293F cells and purified by methods described previously[36,43]. Purity
293 was assessed by blue native polyacrylamide gel electrophoresis (BN-PAGE) and binding
294 reactivity with HIV-1 bnAbs was assessed by ELISA.

295 **Binding analysis of mAbs by ELISA**

296 Briefly, 96-well ELISA plates (Costar) were coated with 5µg/ml recombinant HIV-1 gp120
297 monomeric proteins overnight at 4°C in 0.1 M $NaHCO_3$ (pH 9.6). Next day, plates were
298 washed thrice with 1×PBS (phosphate buffered saline) and blocked with 15% FBS RPMI
299 and 2% BSA. After 1.5 hours of blocking at 37°C, plates were washed thrice with 1×PBS.

300 Then, serial dilutions of monoclonal antibodies (mAbs) were added and incubated for 1
301 hour at 37°C. Next, alkaline phosphatase (AP) labelled anti-Fc secondary antibody
302 (Southern Biotech) at 1:2,000 was added and plates were incubated at 37°C for 1 hour.
303 Plates were then washed thrice with 1×PBS and AP substrate tablets (Sigma) dissolved
304 in diethanolamine (DAE) was added and incubated for 30 min at room temperature in
305 the dark and readout was taken at 405nm. The BG505.SOSIP.664 gp140 trimeric ELISA
306 was performed as described previously[43].

307 **HIV-1 pseudovirus generation**

308 The HIV-1 pseudoviruses were produced in HEK 293T cells as described earlier[15,18] by
309 co-transfecting the full HIV-1 gp160 envelope plasmid and a pSG3ΔEnv backbone
310 plasmid. Briefly, 1×10^5 cells in 2ml complete DMEM (10% fetal bovine serum (FBS) and
311 1% penicillin and streptomycin antibiotics) were seeded per well of a 6 well cell culture
312 plate (Costar) the day prior to co-transfection for HIV-1 pseudovirus generation. For
313 transfection, envelope (1.25µg) to delta envelope plasmid (2.50µg) ratio was 1:2, this
314 complex was made in Opti-MEM (Gibco) with a final volume of 200µl for each well of the
315 6 well plate and incubated for 5 minutes at room temperature. Next, 3µl of PEI-Max
316 transfection reagent (Polysciences) (1mg/ml) was added to this mixture, mixed well and
317 further incubated for 15 min at room temperature. This mixture was then added
318 dropwise to HEK 293T cells supplemented with fresh complete DMEM growth media and
319 incubated at 37°C for 48 hours. Pseudoviruses were then harvested by filtering cell
320 supernatants with 0.45 mm sterile filter (mdi) and stored frozen at −80°C as aliquots.

321 **HIV-1 neutralization assays**

322 The HIV-1 neutralization assays of monoclonal antibodies (mAbs) were done as
323 described earlier[31,44]. Neutralization was measured as a reduction in luciferase gene
324 expression after a single round of infection of TZM-bl cells (NIH AIDS Reagent Program)
325 with HIV-1 envelope pseudoviruses. The $TCID_{50}$ of the HIV-1 pseudoviruses was
326 calculated and 200 $TCID_{50}$ of the virus was used in neutralization assays by incubating
327 with 1:3 serially diluted mAbs starting at 10 µg/ml. After that, freshly trypsinized TZM-
328 bl cells in growth medium (complete DMEM with 10% FBS and 1% penicillin and
329 streptomycin antibiotics) containing 50µg/ml DEAE Dextran and 1 mM Indinavir (in case
330 of primary isolates) at 10^5 cells/well were added and plates were incubated at 37°C for

331 48 hours. Virus controls (cells with HIV-1 virus only) and cell controls (cells without virus
332 and antibody) were included. MuLV was used as a negative control. After the incubation
333 of the plates for 48 hours, luciferase activity was measured using the Bright-Glow
334 Luciferase Assay System (Promega). IC_{50} for antibodies were calculated. Values were
335 derived from a dose-response curve fit with a non-linear function using the GraphPad
336 Prism 9 software (San Diego, CA).

337 **Fab Fragment Preparation**

338 The Fab fragments were generated from 4 mg of 44m IgG antibody using a Fab
339 Fragmentation Kit (G Biosciences) according to manufacturer's protocol. Purity and size
340 of Fab fragments were assessed by SDS-PAGE.

341 **Octet BLI analysis**

342 Octet biolayer interferometry (BLI) was performed using an Octet Red96 instrument
343 (ForteBio, Inc.). A 5 μg/ml concentration of each mAb was captured on a protein A sensor
344 and its binding kinetics were tested with serial 2-fold diluted HIV-1 SOSIP trimer protein
345 (100 nM to 6.25 nM). The baseline was obtained by measurements taken for 60 s in BLI
346 buffer (1x PBS and 0.05% Tween-20), and then, the sensors were subjected to association
347 phase immersion for 300 s in wells containing serial dilutions of HIV-1 SOSIP protein.
348 Then, the sensors were immersed in BLI buffer for as long as 600 s to measure the
349 dissociation phase. The mean Kon, Koff and apparent KD values of the mAbs binding
350 affinities for HIV-1 SOSIP envelope protein were calculated from all the binding curves
351 based on their global fit to a 1:1 Langmuir binding model using Octet software version
352 12.0.

353 **Negative-stain EM**

354 To observe the binding pattern of 44m bnAb to BG505 SOSIP trimer and the homogeneity
355 of the complex, we first performed room temperature negative staining TEM. The SEC
356 purified complex of BG505 SOSIP trimer and 44m bnAb (1.2 mg/ml) was diluted by 70
357 times for analysis. The 3.5 μl of sample mixture was put onto a glow discharged carbon
358 coated Cu grids for 30 secs (EM grid, 300 mesh, Electron Microscopy Sciences). After 1.5
359 min of incubation of the sample on the grid, the remained solvent was blotted and three

360 drops of 1% uranyl acetate (Uranyl Acetate 98%, ACS Reagent, Polysciences, Inc.) was
361 applied on the grid for staining purpose. The excess stain was blotted after each addition
362 and after air dried, the grid was used for data collection with 120 kV Talos L120C electron
363 microscope. Data acquisition was performed using 4k x 4k Ceta camera at the
364 magnification of 73kx and it is calibrated at 3.84Å/pixel. The collected images were
365 processed in EMAN 2.1[45]. From these micrographs we picked particles in both manual
366 and automated mode, and its co-ordinates were extracted using e2boxer.py in EMAN 2.1.
367 Followed by, reference free 2D class averages were performed to analyze different views
368 of bnAb bound trimer complex. The cleaned particles after extraction were taken for
369 reference-free 2D class averages using simple_prime2D of SIMPLE 2.1 software[46] with a
370 mask diameter of 30 pixels at 3.84 Å/pix.

371 **Sample preparation for cryoEM**

372 R1.2/1.3 300 mesh copper grids (Quantifoil) (Electron Microscopy Sciences) were glow
373 discharged at 20mA for 90 seconds before cryo-freezing. Three microliters of the SEC
374 purified complex of BG505 SOSIP trimer and 44m bnAb (1.2 mg/ml) was applied onto the
375 freshly glow discharged grid, and immediately blotted for 8.5 secs without any blot force
376 just after 10 secs of incubation to remove excess solvent in pre-equilibrated chamber of
377 FEI Vitrobot Mark IV plunger. The sample was plunged into the liquid ethane just after
378 blotting.

379 **CryoEM data acquisition**

380 Cryo-EM data were collected using 200 kV TalosArctica transmission electron
381 microscope (Thermo Scientific™) equipped with Gatan K2 Summit Direct Electron
382 Detector. Movies were recorded automatically using Latitude-S (DigitalMicrograph - GMS
383 3.5) at nominal magnification of 45,000x at the effective pixel size of 1.17 Å (*14*).
384 Micrographs were acquired in counting mode with a total dose of 60 e^-/Å2, with an
385 exposure time of 8 sec distributed for 20 frames. A total of 3000 movies were acquired
386 for the BG505 SOSIP trimer and 44m bnAbs protein complexes respectively.

387 **CryoEM data analysis and model building**

388 Single-Particle Analysis (SPA) were performed for the acquired cryo-EM movies using the
389 Relion version 3.1[47]. At first, drift and gain corrections of the individual movies were

390 performed with MotionCorr2[48]and estimated Contrast transfer function (CTF)
391 parameters using CTFFIND 4.1.13[49]. Subsequently, CTF estimated micrographs were
392 subjected to analyze to eliminate bad micrographs using cisTEM[50] and also, to remove
393 poor resolution micrographs with a fit resolution threshold of 7 Å. The particles from best
394 micrographs were chosen for automated picking using 2D reference in Relion and
395 extracted with the box sizes of 280 Å for the BG505 SOSIP trimer and 44m bnAb
396 complexes. After three rounds of rigorous 2D classification good classes with high-
397 resolution features of the complex were obtained as 1080743 particles. These well-
398 defined particles were selected for 3D classification with C3 symmetry. To achieve high
399 resolution, all particles belonging to the best classes of the complex was accounted for 3D
400 auto-refinement and followed by movie refinement. The sharpening for the 3D auto-
401 refined maps was performed with Relion 3.1[47] and PHENIX[51]. Overviews of cryo-EM data
402 processing is shown in **Table S2**. Global resolution of Fourier shell correlation (FSC) was
403 estimated at the threshold of 0.143 and the estimation of local resolution were performed
404 with ResMap, using two auto-refined half maps.

405 Automated model building was iteratively done with Phenix Real Space Refinement. Only
406 the Env trimer (PDB ID: 5aco) was docked with cryo-EM maps using UCSF Chimera "Fit
407 in map" tool. To build the model for bnAb, the query sequences of the Fab was submitted
408 to Swiss-Model and the resultant model was also fitted in the EM maps. The structural
409 statistics for Cryo-EM map and atomic model were analyzed using Phenix[51], EMringer[52],
410 Molprobity[53], and UCSF chimera[54]. Cryo-EM map and atomic model were visualized using
411 UCSF ChimeraX[55].

412 **Quantification and statistical analysis**

413 All statistical analysis was done with GraphPad Prism software version 9.

414 **DATA AVAILABILITY**

415 The sequence of the 44m heavy chain variable region has been deposited in GenBank with
416 accession numbers xxx and xxx respectively. The PDB ID for the EM map of 44m Fab in
417 complexed with BG505.SOSIP.664.C2 T332N gp140 trimer reported in this study is EMD:
418 xxx PDB:xxx .Any additional data are available upon reasonable request from the
419 corresponding authors. Source data are provided in this paper.

ACKNOWLEDGMENTS

This antibody work was supported by Department of Biotechnology, India Indo-SA grant (BT/PR2450/MED/29/1222/2017) and (BT/PR30120/MED/29/1339/2018) grants awarded to K.L. The cryoEM work and consumables were supported by DBT BUILDER PROGRAM (BT/INF/22/SP22/844/2107), DST-FIST (SR/FST/LSII-039/2015) and SERB (SERB-EMR/2016/000608, SERB-IPA/2020/000094) grants awarded to S.D. S.K. is supported through DBT/Wellcome Trust India Alliance Early Career Fellowship grant IA/E/18/1/504307 (S.K.). We are very much thankful to NIH AIDS reagent program for HIV-1 research reagents, Neutralizing antibody consortium (NAC), IAVI, USA for HIV-1 neutralizing antibodies.

AUTHOR CONTRIBUTIONS

Experimental work, data acquisition and analysis of data by S.Ku., S.D.S., A.C., P.B., S.S, S.Ka, R.L., S.D. Conceptualization and implementation by S.Ku., S.D.S., S.D. and K.L. Manuscript writing by S.Ku., S.D.S., A.C., S.D. and K.L. All authors reviewed the manuscript and approved the final version of the manuscript.

COMPETING INTERESTS

All the authors have read and approved the manuscript for publication and declare no competing interests.

438 **REFERENCES**

439 1. Sok, D. & Burton, D. R. Recent progress in broadly neutralizing antibodies to HIV. *Nat.*
440 *Immunol.***19**, 1179–1188 (2018).
441 2. Burton, D. R. & Hangartner, L. Broadly Neutralizing Antibodies to HIV and Their Role
442 in Vaccine Design. *Annu. Rev. Immunol.***34**, 635–659 (2016).
443 3. Euler, Z. & Schuitemaker, H. Cross-reactive broadly neutralizing antibodies: timing is
444 everything. *Front. Immunol.***3**, 215 (2012).
445 4. Simek, M. D. *et al.* Human immunodeficiency virus type 1 elite neutralizers:
446 individuals with broad and potent neutralizing activity identified by using a high-
447 throughput neutralization assay together with an analytical selection algorithm. *J.*
448 *Virol.***83**, 7337–7348 (2009).
449 5. Andrabi, R., Bhiman, J. N. & Burton, D. R. Strategies for a multi-stage neutralizing
450 antibody-based HIV vaccine. *Curr. Opin. Immunol.***53**, 143–151 (2018).
451 6. Burton, D. R. What Are the Most Powerful Immunogen Design Vaccine Strategies?
452 Reverse Vaccinology 2.0 Shows Great Promise. *Cold Spring Harb. Perspect. Biol.***9**,
453 (2017).
454 7. del Moral-Sánchez, I. *et al.* High thermostability improves neutralizing antibody
455 responses induced by native-like HIV-1 envelope trimers. *Npj Vaccines***7**, 1–12 (2022).
456 8. Goo, L., Chohan, V., Nduati, R. & Overbaugh, J. Early development of broadly
457 neutralizing antibodies in HIV-1-infected infants. *Nat. Med.***20**, 655–658 (2014).
458 9. Simonich, C. A. *et al.* HIV-1 Neutralizing Antibodies with Limited Hypermutation from
459 an Infant. *Cell***166**, 77–87 (2016).
460 10. Khan, L. *et al.* Identification of CD4-Binding Site Dependent Plasma Neutralizing
461 Antibodies in an HIV-1 Infected Indian Individual. *PloS One***10**, e0125575 (2015).
462 11. Khan, L. *et al.* Cross-neutralizing anti-HIV-1 human single chain variable
463 fragments(scFvs) against CD4 binding site and N332 glycan identified from a
464 recombinant phage library. *Sci. Rep.***7**, 45163 (2017).
465 12. Fouda, G. G. *et al.* Immunological mechanisms of inducing HIV immunity in infants.
466 *Vaccine***38**, 411–415 (2020).
467 13. Ditse, Z. *et al.* HIV-1 SUBTYPE C INFECTED CHILDREN WITH EXCEPTIONAL
468 NEUTRALIZATION BREADTH EXHIBIT POLYCLONAL RESPONSES TARGETING
469 KNOWN EPITOPES. *J. Virol.* (2018) doi:10.1128/JVI.00878-18.

470 14. Muenchhoff, M., Prendergast, A. J. & Goulder, P. J. R. Immunity to HIV in Early Life.
471 *Front. Immunol.***5**, 391 (2014).
472 15. Mishra, N. *et al.* Viral characteristics associated with maintenance of elite neutralizing
473 activity in chronically HIV-1 clade C infected monozygotic pediatric twins. *J. Virol.*
474 JVI.00654-19 (2019) doi:10.1128/JVI.00654-19.
475 16. Makhdoomi, M. A. *et al.* Evolution of cross-neutralizing antibodies and mapping
476 epitope specificity in plasma of chronic HIV-1-infected antiretroviral therapy-naïve
477 children from India. *J. Gen. Virol.***98**, 1879–1891 (2017).
478 17. Mishra, N. *et al.* Broadly neutralizing plasma antibodies effective against autologous
479 circulating viruses in infants with multivariant HIV-1 infection. *Nat. Commun.***11**,
480 4409 (2020).
481 18. Kumar, S. *et al.* An HIV-1 Broadly Neutralizing Antibody from a Clade C-Infected
482 Pediatric Elite Neutralizer Potently Neutralizes the Contemporaneous and
483 Autologous Evolving Viruses. *J. Virol.***93**, (2019).
484 19. Scheid, J. F. *et al.* Sequence and structural convergence of broad and potent HIV
485 antibodies that mimic CD4 binding. *Science***333**, 1633–1637 (2011).
486 20. Freund, N. T. *et al.* Coexistence of potent HIV-1 broadly neutralizing antibodies and
487 antibody-sensitive viruses in a viremic controller. *Sci. Transl. Med.***9**, (2017).
488 21. Walker, L. M. *et al.* Broad and potent neutralizing antibodies from an African donor
489 reveal a new HIV-1 vaccine target. *Science***326**, 285–289 (2009).
490 22. Walker, L. M. *et al.* Broad neutralization coverage of HIV by multiple highly potent
491 antibodies. *Nature***477**, 466–470 (2011).
492 23. Huang, J. *et al.* Broad and potent neutralization of HIV-1 by a gp41-specific human
493 antibody. *Nature***491**, 406–412 (2012).
494 24. Huang, J. *et al.* Identification of a CD4-Binding-Site Antibody to HIV that Evolved Near-
495 Pan Neutralization Breadth. *Immunity***45**, 1108–1121 (2016).
496 25. Bonsignori, M. *et al.* Staged induction of HIV-1 glycan-dependent broadly neutralizing
497 antibodies. *Sci. Transl. Med.***9**, (2017).
498 26. Falkowska, E. *et al.* Broadly neutralizing HIV antibodies define a glycan-dependent
499 epitope on the prefusion conformation of gp41 on cleaved envelope trimers.
500 *Immunity***40**, 657–668 (2014).
501 27. Schoofs, T. *et al.* Broad and Potent Neutralizing Antibodies Recognize the Silent Face
502 of the HIV Envelope. *Immunity***50**, 1513-1529.e9 (2019).

503 28. Doria-Rose, N. A. *et al.* New Member of the V1V2-Directed CAP256-VRC26 Lineage
504 That Shows Increased Breadth and Exceptional Potency. *J. Virol.***90**, 76–91 (2016).
505 29. Aggarwal, H. *et al.* Alterations in B Cell Compartment Correlate with Poor
506 Neutralization Response and Disease Progression in HIV-1 Infected Children. *Front.*
507 *Immunol.***8**, 1697 (2017).
508 30. Kumar, S. *et al.* CD4-Binding Site Directed Cross-Neutralizing scFv Monoclonals from
509 HIV-1 Subtype C Infected Indian Children. *Front. Immunol.***8**, 1568 (2017).
510 31. Montefiori, D. C. Measuring HIV neutralization in a luciferase reporter gene assay.
511 *Methods Mol. Biol. Clifton NJ***485**, 395–405 (2009).
512 32. Setliff, I. *et al.* Multi-Donor Longitudinal Antibody Repertoire Sequencing Reveals the
513 Existence of Public Antibody Clonotypes in HIV-1 Infection. *Cell Host Microbe***23**, 845-
514 854.e6 (2018).
515 33. Willis, J. R. *et al.* Human immunoglobulin repertoire analysis guides design of vaccine
516 priming immunogens targeting HIV V2-apex broadly neutralizing antibody
517 precursors. *Immunity***0**, (2022).
518 34. Sok, D. *et al.* The effects of somatic hypermutation on neutralization and binding in
519 the PGT121 family of broadly neutralizing HIV antibodies. *PLoS Pathog.***9**, e1003754
520 (2013).
521 35. Bonsignori, M. *et al.* Maturation Pathway from Germline to Broad HIV-1 Neutralizer
522 of a CD4-Mimic Antibody. *Cell***165**, 449–463 (2016).
523 36. Sok, D. *et al.* Recombinant HIV envelope trimer selects for quaternary-dependent
524 antibodies targeting the trimer apex. *Proc. Natl. Acad. Sci. U. S. A.***111**, 17624–17629
525 (2014).
526 37. Julien, J.-P. *et al.* Broadly neutralizing antibody PGT121 allosterically modulates CD4
527 binding via recognition of the HIV-1 gp120 V3 base and multiple surrounding glycans.
528 *PLoS Pathog.***9**, e1003342 (2013).
529 38. Mouquet, H. *et al.* Complex-type N-glycan recognition by potent broadly neutralizing
530 HIV antibodies. *Proc. Natl. Acad. Sci. U. S. A.***109**, E3268-3277 (2012).
531 39. Dingens, A. S., Arenz, D., Weight, H., Overbaugh, J. & Bloom, J. D. An Antigenic Atlas of
532 HIV-1 Escape from Broadly Neutralizing Antibodies Distinguishes Functional and
533 Structural Epitopes. *Immunity***50**, 520-532.e3 (2019).
534 40. Smith, K. *et al.* Rapid generation of fully human monoclonal antibodies specific to a
535 vaccinating antigen. *Nat. Protoc.***4**, 372–384 (2009).

536 41. Lefranc, M.-P. *et al.* IMGT, the international ImMunoGeneTics information system.
537 *Nucleic Acids Res.***37**, D1006-1012 (2009).
538 42. Kumar, S. *et al.* Structural insights for neutralization of Omicron variants BA.1, BA.2,
539 BA.4, and BA.5 by a broadly neutralizing SARS-CoV-2 antibody. *Sci. Adv.***8**, eadd2032
540 (2022).
541 43. Sanders, R. W. *et al.* A next-generation cleaved, soluble HIV-1 Env trimer, BG505
542 SOSIP.664 gp140, expresses multiple epitopes for broadly neutralizing but not non-
543 neutralizing antibodies. *PLoS Pathog.***9**, e1003618 (2013).
544 44. Kumar, S. *et al.* Effect of combination antiretroviral therapy on human
545 immunodeficiency virus 1 specific antibody responses in subtype-C infected children.
546 *J. Gen. Virol.***101**, 1289–1299 (2020).
547 45. Bell, J. M., Chen, M., Baldwin, P. R. & Ludtke, S. J. High resolution single particle
548 refinement in EMAN2.1. *Methods San Diego Calif***100**, 25–34 (2016).
549 46. Reboul, C. F., Eager, M., Elmlund, D. & Elmlund, H. Single-particle cryo-EM-Improved
550 ab initio 3D reconstruction with SIMPLE/PRIME. *Protein Sci. Publ. Protein Soc.***27**, 51–
551 61 (2018).
552 47. Scheres, S. H. W. RELION: Implementation of a Bayesian approach to cryo-EM
553 structure determination. *J. Struct. Biol.***180**, 519–530 (2012).
554 48. Zheng, S. Q. *et al.* MotionCor2: anisotropic correction of beam-induced motion for
555 improved cryo-electron microscopy. *Nat. Methods***14**, 331–332 (2017).
556 49. Rohou, A. & Grigorieff, N. CTFFIND4: Fast and accurate defocus estimation from
557 electron micrographs. *J. Struct. Biol.***192**, 216–221 (2015).
558 50. Grant, T., Rohou, A. & Grigorieff, N. cisTEM, user-friendly software for single-particle
559 image processing. *eLife***7**, e35383 (2018).
560 51. Adams, P. D. *et al.* PHENIX: a comprehensive Python-based system for
561 macromolecular structure solution. *Acta Crystallogr. D Biol. Crystallogr.***66**, 213–221
562 (2010).
563 52. Barad, B. A. *et al.* EMRinger: side chain–directed model and map validation for 3D
564 cryo-electron microscopy. *Nat. Methods***12**, 943–946 (2015).
565 53. Williams, C. J. *et al.* MolProbity: More and better reference data for improved all-atom
566 structure validation. *Protein Sci. Publ. Protein Soc.***27**, 293–315 (2018).
567 54. Pettersen, E. F. *et al.* UCSF Chimera--a visualization system for exploratory research
568 and analysis. *J. Comput. Chem.***25**, 1605–1612 (2004).

569 55. Goddard, T. D. *et al.* UCSF ChimeraX: Meeting modern challenges in visualization and
570 analysis. *Protein Sci. Publ. Protein Soc.* **27**, 14–25 (2018).

571

572 **FIGURES WITH FIGURE LEGENDS**

573
574
575
576
577
578
579
580
581
582
583
584
585
586

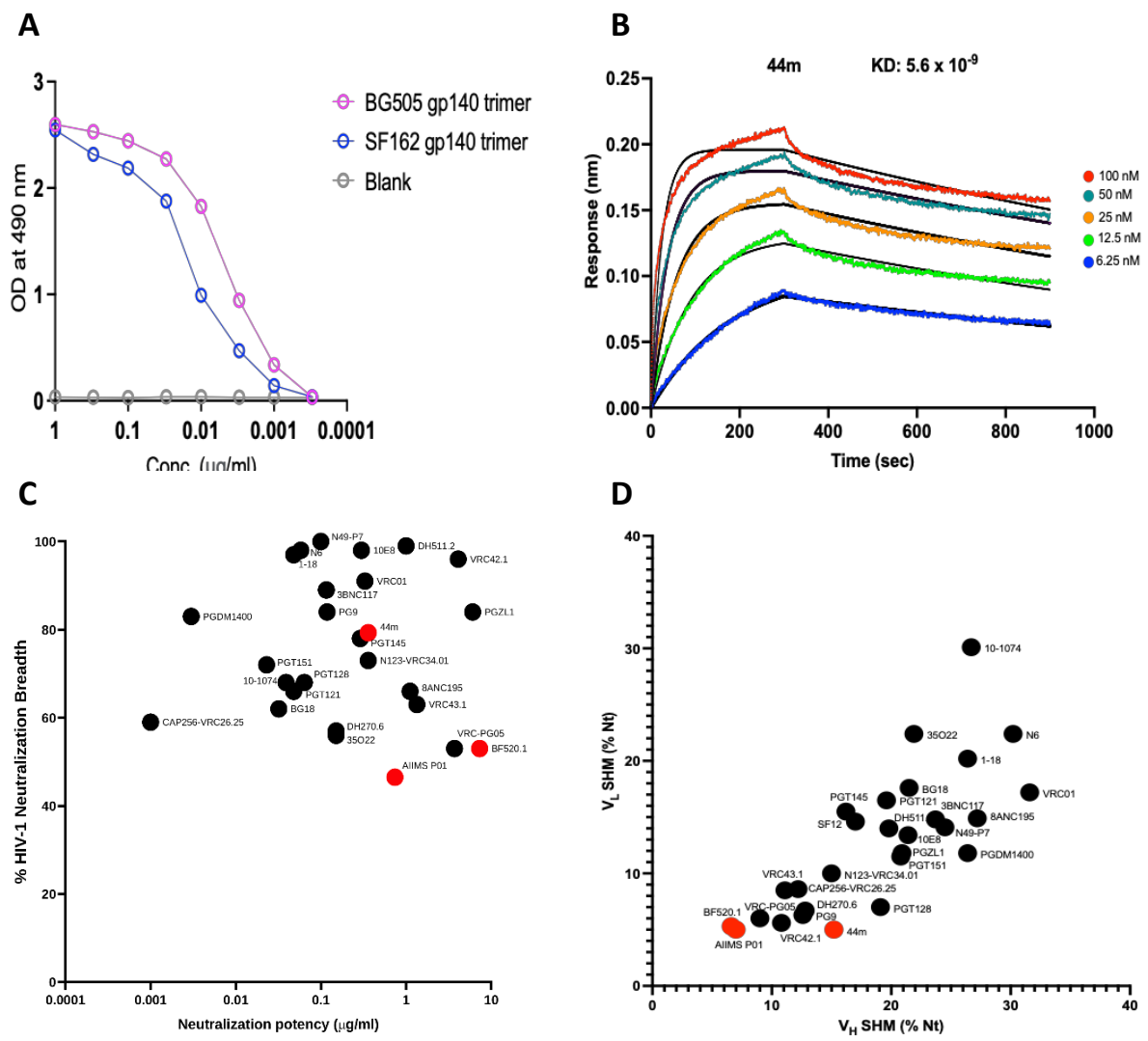

587 **Figure 1: Binding Reactivity and Affinity of matured 44m bnAb to heterologous**
588 **HIV-1 envelope glycoproteins. (A)** Antigen Binding reactivity of the 44m mAb to
589 heterologous HIV-1 trimeric envelope proteins determined by ELISA. **(B)** Binding Affinity
590 of 44m to BG505 envelope trimer determined by Octet BLI. **(C)** Neutralization breadth
591 comparison of HIV-1 adult and pediatric bnAbs is shown. **(D)** Somatic hypermutation
592 (SHM) analysis of HIV-1 adult and pediatric bnAbs shown as % nucleotide (Nt) mutations
593 relative to respective germline variable gene sequence. Here, pediatric HIV-1 bnAbs are
594 highlighted in red color.

A

Global Panel					
S.No.	Virus ID	Tier	Clade	AIIMS_P01	AIIMS_P01_44
1	CNE55	3	AE	>10	>10
2	TRO11	2	B	1.5	1.15
3	CNE8	2	AE	>10	>10
4	CH119	2	BC	0.75	0.45
5	25710	1B	C	1.2	0.7
6	X2278	2	B	5.7	1.41
7	246F3	3	A/C	> 10	>10
8	X1632	2	G	>10	>10
9	CE1176	2	C	0.8	0.26
10	398F1	2	A	0.25	0.16
11	CEO217	3	C	>10	>10
12	BJOX 2000	2	BC	0.25	0.15
			GMT	0.87	0.43
			Breath	58%	58%

B

S.No.	Virus ID	Tier	Clade	AIIMS_P01	AIIMS_P01_44
1	QB726.70.M env C4	1B	A	>10	0.15
2	Q769.ENV H5	1B	A	>10	0.6
3	700010058.A4.4375	1B	B	2.5	0.35
4	SF162	1A	B	0.023	0.022
5	CAAN	2	B	1.55	0.1
6	WITO	2	B	>10	>10
7	TRJO	3	B	>10	>10
8	RHPA	2	B	4.1	0.5
9	TR011	2	B	3	0.2
10	AC10	2	B	>10	0.65
11	QHO692	2	B	>10	2.7
12	SC422661.8	2	B	4.65	0.95
13	1012.TC21.3257	1B	B	>10	0.6
14	1059_09.A4.1460	2	B	>10	9.55
15	PRB931_06.TC3.4930	1B	B	0.4	0.05
16	6244_13.B5.4576	2	B	9.4	0.9
17	6240_08.TA5.4622	2	B	2.1	0.2
18	63358.p3.4013	2	B	>10	0.3
19	THRO	2	B	>10	>10
20	PRB958_06.TB1.4305	2	B	3.1	0.35
21	SC45.4B5.2631	2	B	>10	0.25
22	WEAUd15.410.5017	2	B	3.05	0.2
23	REJO	2	B	>10	>10
24	ZM197	1B	C (African)	>10	>10
25	ZM214	2	C (African)	>10	>10
26	ZM233	2	C (African)	1	0.07
27	ZM53	2	C (African)	>10	>10
28	ZM109	1B	C (African)	>10	>10
29	ZM249	2	C (African)	>10	>10
30	QC406 envF3	2	C (African)	0.55	0.01
31	CAP45	2	C (African)	>10	>10
32	CAP210	2	C (African)	>10	>10
33	Du156	2	C (African)	0.15	0.25
34	Du172	2	C (African)	1.93	1.18
35	Du422.1	2	C (African)	1.21	0.41
36	MJ412	2	C (African)	0.031	0.054
37	16055	2	C (Indian)	>10	>10
38	25710	1	C (Indian)	1.2	0.7
39	25711	1B	C (Indian)	0.033	0.086
40	25925	1B	C (Indian)	0.107	0.04
41	26191	2	C (Indian)	>10	4.75
42	836	1A	C (Indian)	>10	0.01
43	16936	2	C (Indian)	1.4	5.55
44	70606F	ND	C (Indian)	>10	3
45	70607Z	ND	C (Indian)	>10	3.8
46	70607B	ND	C (Indian)	>10	0.6
47	70606B	ND	C (Indian)	9.95	0.9
48	70604B	ND	C (Indian)	9.93	0.75
49	70607C	ND	C (Indian)	>10	1.2
50	70406	ND	C (Indian)	>10	3.4
51	70408	ND	C (Indian)	>10	3.25
52	70402	ND	C (Indian)	>10	1.65
53	709316B	ND	C (Indian)	>10	3.3
54	UZ12A	ND	C (Indian)	>10	1.55
55	329.14.B1	2	C (Indian)	0.035	0.03
56	330.16.E6	2	C (Indian)	0.163	0.078
57	MK184	2	CD	0.79	0.04
58	BK184	2	CD	0.05	0.02
GMT				0.74	0.36
Breadth				46.50%	79.30%

IC50 Color code (ug/ml)
< 1
14
5-10
>10

Figure 2: Matured AIIMS-P01 lineage antibody 44m showed broad HIV-1 neutralization with improved potency. (A) Heat map depicting IC_{50} values of the matured 44m mAb tested against HIV-1 global panel. **(B)** Heat map depicting IC50 values of the 44m tested against heterologous panel of HIV-1 viruses, using a TZM-bl based neutralization assay (n=58).

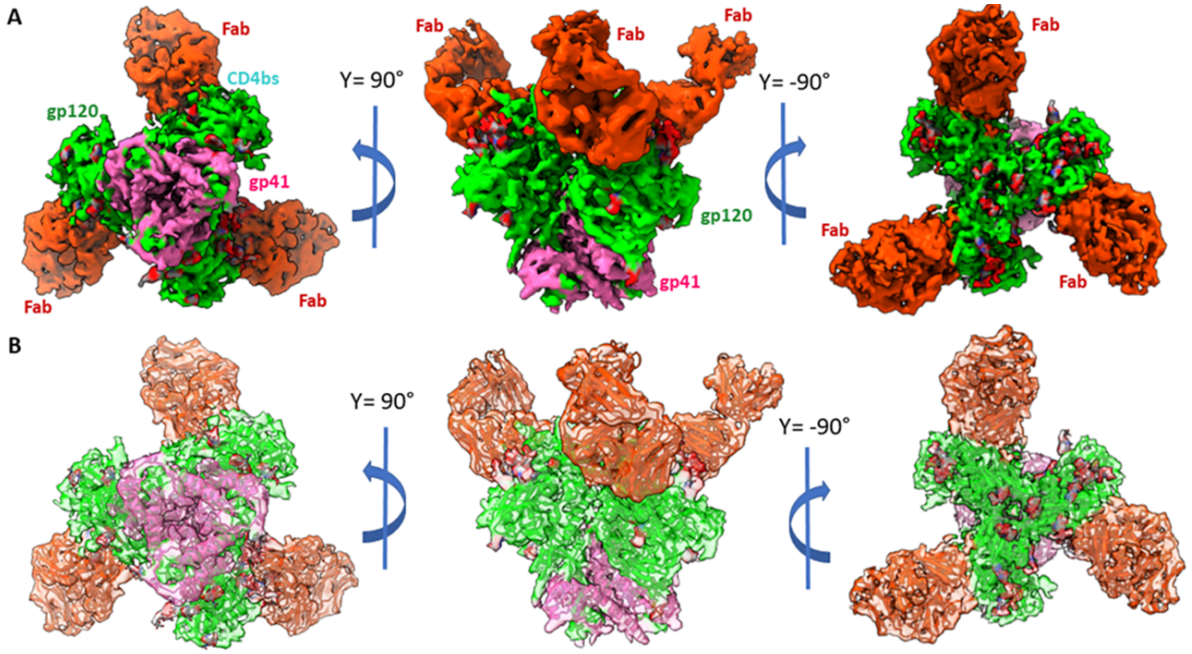

Figure 3: Cryo-EM reconstruction and model of BG505.SOSIP trimer in complex with 44m bnAb. (A) Side and top views of Cryo-EM reconstructed map of BG505.SOSIP trimer in complex with 44m bnAb solved at ~4.4Å resolution, with a local resolution in between 3.36 and 3.74Å. Color coding corresponding to segmented EM densities are: orange red, 44m bnAb; lime green, gp120; pink, gp41. **(B)** The corresponding atomic model fitted in the EM map of BG505 trimer in complex with 44m bnAb showing three 44m bnAb binds to each gp120 monomeric subunit for effective neutralization.

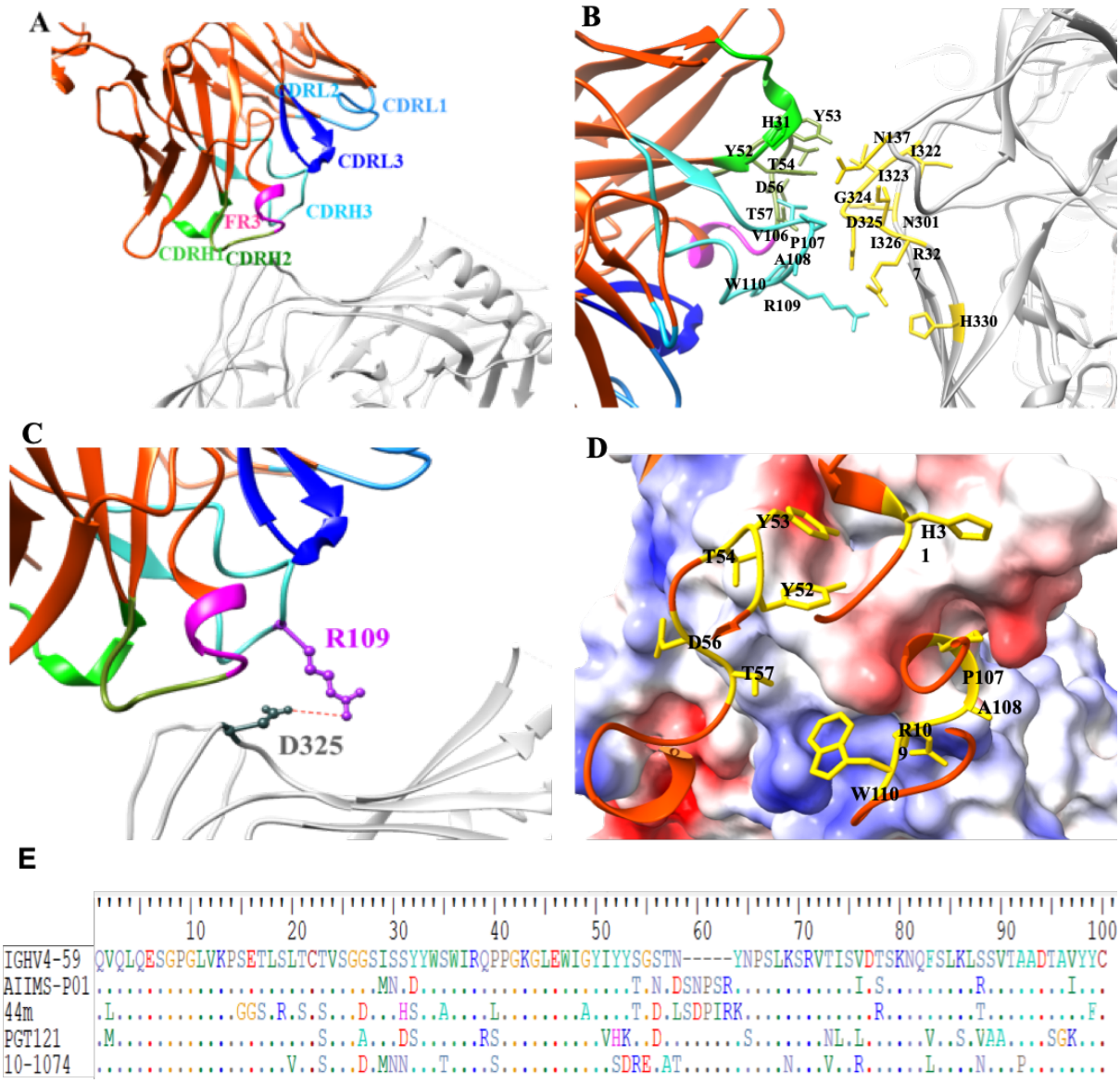

Figure 4: Interaction sites for 44m bnAb to form a complex with BG505 SOSIP trimer. (A) The CDR regions in the interface of gp120 and 44m bnAb are highlighted using color coding: magenta, FR3; green, CDRH1, olive green, CDRH2; and, cyan, CDRH3; dodger blue, CDRL1; deep sky blue, CDRL2; median blue, CDRL3. **(B)** Salt bridge interaction in between D325 residue in the V loop of gp120 monomer and CDRH1 region, where D325 is shown in dark green and R109 is shown in purple color, and the bond is shown in red color. **(C)** Different interacting partners in the epitope region to adapt a stable conformational state with the CDR regions. **(D)** Electrostatic potential surface map of the interacting region of gp120 showing the interacting residues of the paratope facing towards the charged residues of the epitope. The residues on 44m bnAb is shown in golden color. **(E)** Heavy chain sequence alignment of 44m bnAb with other V3-glycan bnAbs belong to IGHV4-59 gene.

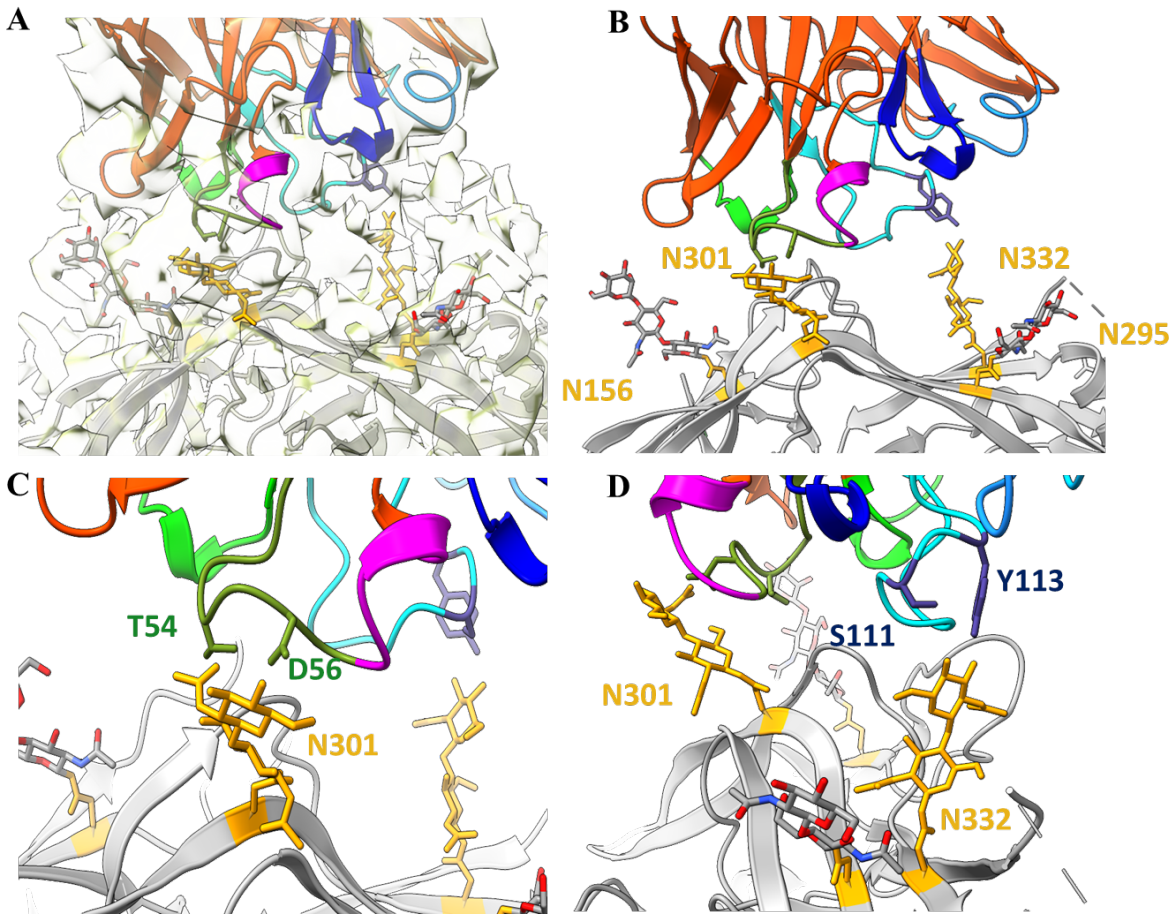

Figure 5: Glycan interaction sites of BG505.SOSIP trimer in complex with 44m Fab. **(A)** Positions and fitting different glycan residues are pointed in the EM map shown. In the atomic model N301 and N332 glycans are shown in orange color, whereas the Fab and CDR regions are colored similarly to Figure 2. **(B)** The gp120 monomer is shown in gray. Atomic model illustrating various glycan residues interacting with different region of CDR regions of 44m bnAb, where glycan attached to N156 is coming closer to CDRH1 region. **(C)** The NAG attached to Asn301 is making contact points with Thr54 and Asp56 in the CDRH2 region (shown in olive drab color). **(D)** Glycan binding to Asn332 is interacting with Ser111 and Tyr113 residues of the CDRH3 region (shown in deep blue color).